Monthly Notices
of the
ROYAL ASTRONOMICAL SOCIETY

Mon. Not. R. Astron. Soc. **403,** 1577–1591 (2010) doi:10.1111/j.1365-2966.2010.16221.x

Polarization towards the young open cluster NGC 6823

Biman J. Medhi,[1★] Maheswar G.,[1] J. C. Pandey,[1] Motohide Tamura[2] and R. Sagar[1]

[1]*Aryabhatta Research Institute of Observational Sciences (ARIES), Manora Peak, Nainital 263 129, India*
[2]*National Astronomical Observatory of Japan, Mitaka, Tokyo 181-8588, Japan*

Accepted 2009 December 16. Received 2009 December 9; in original form 2009 September 11

ABSTRACT

We present multiwavelength linear polarimetric observations of 104 stars towards the region of young open cluster NGC 6823. The polarization towards NGC 6823 is dominated by foreground dust grains and we found evidence for the presence of several layers of dust towards the line of sight. The first layer of dust is approximately located within 200 pc towards the cluster, which is much closer to the Sun than the cluster itself (∼2.1 kpc). The radial distribution of the position angles for the member stars is found to show a systematic change, while the polarization is found to reduce towards the outer parts of the cluster and the average position angle of the coronal region of the cluster is very close to the inclination of the Galactic parallel (∼32°). The size distribution of the grains within NGC 6823 is similar to those in the general interstellar medium. The patchy distribution of foreground dust grains is suggested to be mainly responsible for both differential reddening and polarization towards NGC 6823. The majority of the observed stars do not show evidence of intrinsic polarization in their light.

Key words: polarization – dust, extinction – open clusters and associations: individual: NGC 6823.

1 INTRODUCTION

The polarization of starlight through selective extinction by aligned/partially aligned and asymmetric dust grains present in the general interstellar medium can be considered as a valuable tool to study both the grain properties, such as size and shape, and the small-/large-scale structure of interstellar magnetic fields in different lines of sight. Although the identity of the dominant grain-alignment mechanism has proved to be an intriguing problem in grain dynamics (Lazarian, Goodman & Myers 1997), it is generally believed that asymmetric grains tend to become aligned to the local magnetic field with their shortest axis parallel to the field. For this orientation, the observed polarization vector is parallel to the plane-of-sky projection of a line-of-sight-averaged magnetic field (Davis & Greenstein 1951). Interstellar polarization varies strongly with wavelength (Serkowski, Mathewson & Ford 1975; Wilking, Lebofsky & Rieke 1982). In particular, the wavelength of maximum interstellar polarization ($\lambda_{\rm max}$) is thought to be related to the total-to-selective extinction (R_V) as $R_V = (5.6 \pm 0.3)\lambda_{\rm max}$ (Whittet & van Breda 1978). Generally, unreddened stars show no polarization if they are not sources of intrinsic polarization. For stars with large colour excess [$E(B-V)$], the values of polarization P show a wide distribution given by $P/E(B-V)_{\rm max} = 0.090\,{\rm mag}^{-1}$, where P is measured at a visual wavelength (Spitzer 1978).

The polarimetric study of young open clusters can provide us with valuable information about foreground interstellar dust, because of the available knowledge of their physical parameters such as distance, membership probability ($M_{\rm P}$) and colour excess. As part of an observational programme to carry out polarimetric observations of young open clusters, in order to investigate properties such as magnetic field orientation $\lambda_{\rm max}$, maximum polarization $P_{\rm max}$, etc. (Medhi et al. 2007, 2008), we observed the young open cluster NGC 6823, which is a *Hubble Space Telescope* (*HST*) polarimetric calibration object (Turnshek et al. 1990). The young open cluster NGC 6823 [RA(J2000) $19^{\rm h}43^{\rm m}09^{\rm s}$, Dec.(J2000) $+23^\circ18^{\rm m}00^{\rm s}$; $l = 59.402, b = -0.144$] is the central cluster of the Vul OBI association (Morgan, Whitford & Code 1953). It is located in the local arm (Orion) of our Galaxy. A distance modulus of 11.6 ± 0.01 mag, which corresponds to a distance of 2.1 ± 0.1 kpc, is estimated for the cluster (Guetter 1992). The bright main-sequence stars in NGC 6823 reveal an age of ∼5 Myr for the cluster, whereas the pre-main-sequence stars indicate an age lower than 0.3 Myr (Sagar & Joshi 1981).

To study the interstellar polarization in different directions for our Galaxy, Hiltner (1956), Hall (1958) and Serkowski (1965) made polarimetric measurements of a few bright stars in the direction of NGC 6823. The four bright stars observed by Hiltner (1956) and Hall (1958), using Corning 3385 (equivalent to a V filter) and without a filter (clear), respectively, are common and belong to O and B spectral types. Serkowski (1965) had observed 21 stars in the V filter and 17 stars in the B filter, including three bright stars observed by Hiltner (1956) and Hall (1958). However they made

★E-mail: biman@aries.res.in

the observations in survey mode, and therefore no firm conclusions could be drawn from their study.

In this paper, we present the results of polarimetric measurements made for 104 stars in B, V and R_C photometric bands toward NGC 6823 (brighter than $V \simeq 17$ mag). Out of the 104 stars observed, 42 of them have high membership probability ($M_P \geq 0.5$). The paper is organized as follows: in Section 2 we present observations and data reduction, our results and discussion are presented in Section 3 and in Section 4 we conclude with a summary.

2 OBSERVATIONS AND DATA REDUCTION

The polarimetric data for the four fields (centred at RA $19^h43^m10^s$, Dec. + $23°17^m55^s$; RA $19^h43^m24^s$, Dec. + $23°12^m26^s$; RA $19^h43^m24^s$, Dec. + $23°23^m55^s$ and RA $19^h42^m4^s$, Dec. + $23°17^m43^s$) in NGC 6823 were acquired using the ARIES Imaging Polarimeter (AIMPOL: Medhi et al. 2007) mounted on the Cassegrain focus of the 104-cm Sampurnanand Telescope of ARIES, Nainital in B, V and R_c photometric bands, on 2007 May 24, May 25, June 6 and June 7. The imaging was done using a TK 1024 × 1024 pixel^2 CCD camera. Each pixel of the CCD corresponds to 1.7 arcsec and the field of view is ∼8 arcmin diameter on the sky. The full width at half-maximum (FWHM) of the stellar image varies from 2–3 pixel. The read-out noise and gain of the CCD are 7.0 e$^-$ and 11.98 e$^-$ ADU^{-1}, respectively. The fluxes for all of our programme stars were extracted by aperture photometry after bias subtraction in the standard manner using IRAF. Instead of a robust flat-fielding technique we used equation (3) to create a uniform response, as detailed below.

AIMPOL consists of a half-wave plate and a Wollaston prism analyser placed in the telescope beam path to produce ordinary and extraordinary images in slightly different directions separated by ∼27 pixel. To re-image the telescope focal plane on the surface of the CCD, a focal reducer (85 mm, $f/1.8$) is placed between the Wollaston prism and the CCD camera, with a reduction factor of about 4.7.

By definition, the ratio $R(\alpha)$ is given by

$$R(\alpha) = \frac{I_e/I_o - 1}{I_e/I_o + 1} = P\cos(2\theta - 4\alpha), \quad (1)$$

which is the difference between the intensities of the ordinary (I_o) and extraordinary (I_e) beams from their sum. P is the fraction of the total light in the linearly polarized condition and θ is the position angle of the plane of polarization. It is denoted by the normalized Stokes parameter $q\,(= Q/I)$ when the fast axis of the half-wave plate is aligned to the reference axis ($\alpha = 0°$). Similarly, the normalized Stokes parameters $u\,(= U/I)$, $q_1\,(= Q_1/I)$, $u_1\,(= U_1/I)$ are also equivalent to the ratio $R(\alpha)$, when the half-wave plate is at 22°.5, 45° and 67°.5, respectively. In principle, P and θ can be determined by using only two Stokes parameters q and u. In reality, the situation is not so simple for two reasons: (i) the responsiveness of the system to the two orthogonal polarization components may not be same and (ii) the responsiveness of the CCD is a function of position on its surface. The signals that are actually measured in the two images (I'_o and I'_e) may therefore differ from the observed one by the following formula (Ramaprakash et al. 1998):

$$\frac{I_e(\alpha)}{I_o(\alpha)} = \frac{I'_e(\alpha)}{I'_o(\alpha)} \times \frac{F_o}{F_e}, \quad (2)$$

and equation (1) can be rewritten as

$$R(\alpha) = \frac{(I'_e/I'_o \times F_o/F_e) - 1}{(I'_e/I'_o \times F_o/F_e) + 1} = P\cos(2\theta - 4\alpha), \quad (3)$$

Table 1. Observed polarized and unpolarized standard stars.

	Polarized Standard				Unpolarized Standard	
Filter	$P \pm \epsilon$(per cent)	$\theta \pm \epsilon(°)$	$P \pm \epsilon$(per cent)	$\theta \pm \epsilon(°)$	q(per cent)	u(per cent)
	Schmidt et al. (1992)		This work		This work	
	Hiltner-960				**HD21447**	
B	5.72 ± 0.06	55.06 ± 0.31	5.69 ± 0.20	55 ± 2	0.019	0.011
V	5.66 ± 0.02	54.79 ± 0.11	5.61 ± 0.14	53 ± 2	0.037	−0.031
R	5.21 ± 0.03	54.54 ± 0.16	5.20 ± 0.06	54 ± 2	−0.035	−0.039
	HD 204827				**HD12021**	
B	5.65 ± 0.02	58.20 ± 0.11	5.72 ± 0.09	59 ± 2	−0.081	0.071
V	5.32 ± 0.02	58.73 ± 0.08	5.35 ± 0.03	60 ± 2	0.042	−0.045
R	4.89 ± 0.03	59.10 ± 0.17	4.90 ± 0.20	59 ± 2	0.020	0.031
	BD+64°106				**HD14069**	
B	5.51 ± 0.09	97.15 ± 0.47	5.46 ± 0.10	99 ± 2	0.038	−0.010
V	5.69 ± 0.04	96.63 ± 0.18	5.58 ± 0.11	97 ± 2	0.021	0.018
R	5.15 ± 0.10	96.74 ± 0.54	5.20 ± 0.02	97 ± 2	0.010	−0.014
	HD 19820				**G191B2B**	
B	4.70 ± 0.04	115.70 ± 0.22	4.75 ± 0.20	114 ± 2	0.072	−0.059
V	4.79 ± 0.03	114.93 ± 0.17	4.81 ± 0.10	114 ± 2	−0.022	−0.041
R	4.53 ± 0.03	114.46 ± 0.17	4.65 ± 0.13	113 ± 2	−0.036	0.027

		Secondary Polarized Standard			
Star Name	Filter	$P \pm \epsilon$(per cent)	θ	$P \pm \epsilon$(per cent)	$\theta \pm \epsilon(°)$
		Turnshek et al. (1990)		This work	
NGC 6823-2j	V	2.67 ± 0.11	13.0	2.70 ± 0.01	11 ± 2
NGC 6823-6j	V	3.23 ± 0.13	09.0	3.24 ± 0.07	08 ± 2
NGC 6823-7j	V	3.74 ± 0.13	06.9	3.74 ± 0.15	06 ± 2
NGC 6823-10j	V	4.55 ± 0.13	07.2	4.57 ± 0.01	06 ± 2

Table 2. Observed B, V and R_c polarization values for different stars in NGC 6823.

ID(M)† (1)	ID(B)†† (2)	V(mag) (3)	$P_B \pm \epsilon$ (per cent) (4)	$\theta_B \pm \epsilon$ (°) (5)	$P_V \pm \epsilon$(per cent) (6)	$\theta_V \pm \epsilon$ (°) (7)	$P_R \pm \epsilon$ (per cent) (8)	$\theta_R \pm \epsilon$ (°) (9)	$M_P(E)$* (10)	$M_P(D)$** (11)
01	–	16.06	1.93 ± 0.54	26 ± 9	2.15 ± 0.32	32 ± 5	1.88 ± 0.17	25 ± 4	–	–
02	20	14.98	4.13 ± 0.16	2 ± 2	4.39 ± 0.09	2 ± 2	4.28 ± 0.11	4 ± 2	0.96	0.86
03	74	13.77	2.56 ± 0.05	9 ± 2	2.70 ± 0.01	11 ± 2	2.55 ± 0.03	9 ± 2	0.97	0.72
04	73	11.47	0.50 ± 0.07	23 ± 8	0.52 ± 0.09	25 ± 5	0.51 ± 0.01	22 ± 3	–	–
05	18	16.36	3.47 ± 0.18	9 ± 2	3.34 ± 0.55	12 ± 5	3.54 ± 0.23	5 ± 2	–	0.00
06	23	16.29	2.32 ± 0.70	22 ± 5	2.51 ± 0.14	22 ± 2	2.47 ± 0.07	26 ± 2	–	0.88
07	17	14.2	3.72 ± 0.01	4 ± 2	3.74 ± 0.15	6 ± 2	3.73 ± 0.03	5 ± 2	0.97	0.77
08	78	14.27	3.15 ± 0.03	2 ± 2	3.69 ± 0.07	4 ± 2	3.44 ± 0.08	2 ± 2	0.93	0.80
09	–	16.25	4.17 ± 0.21	4 ± 2	4.10 ± 0.30	5 ± 2	4.12 ± 0.08	3 ± 2	–	0.83
10	27	15.05	1.97 ± 0.01	23 ± 2	2.18 ± 0.14	27 ± 2	2.11 ± 0.15	22 ± 3	–	0.01
11	26	13.86	1.99 ± 0.07	18 ± 2	1.98 ± 0.06	20 ± 2	1.88 ± 0.03	16 ± 2	–	0.00
12	13	11.98	3.06 ± 0.09	8 ± 2	3.13 ± 0.06	12 ± 2	3.06 ± 0.04	8 ± 2	0.95	0.81
13	28	16.4	3.42 ± 0.52	3 ± 4	3.78 ± 0.49	5 ± 4	3.79 ± 0.04	8 ± 2	–	0.88
14	75	15.19	2.13 ± 0.16	23 ± 2	2.15 ± 0.17	23 ± 3	2.20 ± 0.05	24 ± 2	–	0.88
15	77	15.13	1.63 ± 0.03	21 ± 2	1.72 ± 0.03	27 ± 2	1.66 ± 0.29	33 ± 6	–	0.45
16	76	15.78	3.12 ± 0.15	5 ± 2	3.24 ± 0.07	8 ± 2	3.19 ± 0.01	5 ± 2	–	0.84
17	16	16.06	3.15 ± 0.11	3 ± 2	3.73 ± 0.31	5 ± 2	3.08 ± 0.28	4 ± 3	–	–
18	71	15.67	0.98 ± 0.18	26 ± 7	1.24 ± 0.10	17 ± 3	1.01 ± 0.08	17 ± 3	–	0.34
19	70	16.49	4.01 ± 0.29	3 ± 2	4.09 ± 0.16	4 ± 2	3.85 ± 0.41	7 ± 3	–	0.89
20	68	13.93	4.50 ± 0.06	4 ± 2	4.57 ± 0.01	6 ± 2	4.48 ± 0.20	4 ± 2	0.96	0.81
21	12	16.26	0.62 ± 0.03	168 ± 3	0.80 ± 0.17	174 ± 4	0.66 ± 0.13	179 ± 3	–	0.00
22	11	13.54	5.04 ± 0.08	3 ± 2	5.28 ± 0.05	4 ± 2	4.94 ± 0.03	2 ± 2	0.97	0.82
23	4	13.63	0.52 ± 0.05	23 ± 9	0.55 ± 0.04	23 ± 9	0.53 ± 0.05	24 ± 8	–	0.00
24	9	13.79	4.46 ± 0.04	12 ± 2	4.40 ± 0.03	13 ± 2	4.22 ± 0.13	12 ± 2	0.97	0.77
25	8	15.82	1.79 ± 0.19	29 ± 3	1.83 ± 0.06	19 ± 2	1.81 ± 0.09	26 ± 2	–	0.82
26	5	14.88	1.49 ± 0.20	26 ± 4	1.82 ± 0.15	35 ± 3	1.41 ± 0.21	40 ± 6	–	0.72
27	64a	14.5	3.33 ± 0.37	96 ± 3	3.39 ± 0.32	98 ± 3	3.25 ± 0.07	94 ± 2	–	0.00
28	65	15.56	5.21 ± 0.51	7 ± 3	5.07 ± 0.17	4 ± 2	4.97 ± 0.10	2 ± 2	–	0.76
29	64	15.07	0.86 ± 0.23	21 ± 8	0.83 ± 0.10	18 ± 7	0.80 ± 0.05	20 ± 4	–	0.00
30	62	14.63	1.34 ± 0.24	26 ± 6	1.44 ± 0.27	28 ± 7	1.39 ± 0.31	23 ± 8	0.95	0.82
31	61	15.49	0.95 ± 0.13	27 ± 7	0.94 ± 0.16	21 ± 4	0.91 ± 0.18	21 ± 7	–	0.41
32	63	16.31	1.40 ± 0.22	15 ± 6	1.42 ± 0.23	20 ± 9	1.44 ± 0.29	24 ± 8	–	0.59
33	65a	16.09	1.19 ± 0.24	17 ± 7	1.22 ± 0.28	17 ± 9	1.27 ± 0.22	16 ± 7	–	0.77
34	–	16.51	0.94 ± 0.18	35 ± 7	1.23 ± 0.21	42 ± 7	0.99 ± 0.17	32 ± 8	–	0.87
35	25	16.48	3.68 ± 0.22	2 ± 3	3.73 ± 0.11	6 ± 2	3.99 ± 0.26	4 ± 6	–	0.89
36	–	16.44	3.03 ± 0.25	8 ± 2	3.03 ± 0.39	7 ± 4	2.83 ± 0.31	4 ± 3	–	–
37	10	16.44	5.94 ± 0.18	9 ± 2	5.50 ± 0.93	9 ± 6	5.55 ± 0.18	12 ± 2	–	0.48
38	–	16.71	3.47 ± 0.23	12 ± 2	3.71 ± 0.65	16 ± 5	3.41 ± 0.22	18 ± 2	–	0.45
39	–	16.43	4.88 ± 0.09	15 ± 2	4.92 ± 0.15	13 ± 2	4.83 ± 0.06	12 ± 2	–	0.89
40	14	14.17	2.88 ± 0.06	2 ± 2	3.31 ± 0.05	3 ± 2	2.97 ± 0.06	3 ± 2	0.97	0.85
41	33	14.99	0.99 ± 0.14	16 ± 9	1.06 ± 0.18	18 ± 8	1.01 ± 0.13	11 ± 5	0.82	0.83
42	36	15.71	2.26 ± 0.21	25 ± 4	2.42 ± 0.23	31 ± 3	2.35 ± 0.05	27 ± 2	–	0.57
43	–	16.77	2.29 ± 0.67	30 ± 8	2.34 ± 0.54	32 ± 7	2.27 ± 0.42	35 ± 5	–	–
44	34	13.91	3.52 ± 0.10	9 ± 2	3.65 ± 0.16	10 ± 2	3.55 ± 0.03	10 ± 2	0.98	0.59
45	51	16.06	1.91 ± 0.20	11 ± 4	2.10 ± 0.11	18 ± 2	1.96 ± 0.17	16 ± 2	–	0.01
46	53	16.09	1.79 ± 0.30	15 ± 6	1.85 ± 0.28	19 ± 5	1.76 ± 0.06	18 ± 2	–	0.02
47	35	11.37	1.52 ± 0.02	29 ± 2	1.63 ± 0.09	29 ± 2	1.47 ± 0.10	28 ± 2	0.79	–
48	50	14.32	0.55 ± 0.02	42 ± 2	0.62 ± 0.08	44 ± 9	0.58 ± 0.06	38 ± 7	–	–
49	49	15.49	1.16 ± 0.13	17 ± 4	1.09 ± 0.06	18 ± 2	1.09 ± 0.10	11 ± 4	–	–
50	–	16.48	1.65 ± 0.36	26 ± 7	1.76 ± 0.36	33 ± 7	1.78 ± 0.22	35 ± 4	–	–
51	42	13.92	0.88 ± 0.16	12 ± 9	0.98 ± 0.01	15 ± 2	0.95 ± 0.01	13 ± 2	–	–
52	98	14.38	1.35 ± 0.39	17 ± 8	1.44 ± 0.31	19 ± 5	1.47 ± 0.32	17 ± 3	–	0.00
53	99	16.01	2.52 ± 0.47	24 ± 4	2.75 ± 0.28	26 ± 3	2.46 ± 0.14	22 ± 4	–	0.00
54	80	14.27	1.75 ± 0.07	17 ± 2	2.15 ± 0.25	20 ± 4	1.83 ± 0.12	18 ± 4	–	0.69
55	79	15.37	3.02 ± 0.15	21 ± 2	3.20 ± 0.64	21 ± 2	3.11 ± 0.66	27 ± 2	–	0.82
56	–	15.57	3.16 ± 0.18	10 ± 2	3.39 ± 0.52	13 ± 5	3.26 ± 0.33	11 ± 2	–	0.02
57	81	14.32	4.02 ± 0.21	172 ± 2	4.54 ± 0.11	176 ± 2	3.93 ± 0.15	170 ± 5	–	–
58	–	16.70	1.96 ± 0.37	28 ± 9	2.26 ± 0.27	29 ± 4	2.01 ± 0.26	24 ± 4	–	0.73
59	82	13.29	0.87 ± 0.13	19 ± 6	0.91 ± 0.08	19 ± 5	0.85 ± 0.04	18 ± 4	0.55	–
60	125	15.01	0.61 ± 0.10	24 ± 8	0.79 ± 0.08	28 ± 6	0.68 ± 0.04	26 ± 5	–	–
61	–	15.43	2.35 ± 0.25	16 ± 9	2.89 ± 0.20	21 ± 6	2.65 ± 0.22	17 ± 2	–	0.29
62	–	12.19	0.59 ± 0.04	37 ± 4	0.67 ± 0.07	38 ± 6	0.63 ± 0.11	34 ± 4	–	–

Table 2 – *continued*

ID(M)† (1)	ID(B)†† (2)	V(mag) (3)	$P_B \pm \epsilon$(per cent) (4)	$\theta_B \pm \epsilon$ (°) (5)	$P_V \pm \epsilon$(per cent) (6)	$\theta_V \pm \epsilon$ (°) (7)	$P_R \pm \epsilon$(per cent) (8)	$\theta_R \pm \epsilon$ (°) (9)	$M_P(E)^*$ (10)	$M_P(D)^{**}$ (11)
63	96	15.06	1.73 ± 0.39	12 ± 3	1.68 ± 0.33	13 ± 4	1.64 ± 0.20	10 ± 3	–	0.00
64	–	15.82	2.85 ± 0.42	6 ± 5	3.20 ± 0.45	9 ± 4	2.79 ± 0.14	7 ± 5	–	–
65	–	16.29	4.80 ± 0.34	41 ± 3	4.86 ± 0.34	38 ± 3	4.77 ± 0.32	36 ± 4	–	–
66	–	15.08	1.65 ± 0.45	8 ± 9	1.63 ± 0.14	13 ± 3	1.55 ± 0.23	12 ± 3	–	–
67	88	14.12	0.65 ± 0.10	6 ± 5	0.72 ± 0.05	8 ± 4	0.66 ± 0.04	7 ± 4	–	0.40
68	–	15.65	1.35 ± 0.20	36 ± 3	1.39 ± 0.17	37 ± 2	1.27 ± 0.17	36 ± 3	–	0.58
69	86	14.50	0.95 ± 0.30	23 ± 6	1.21 ± 0.18	25 ± 6	1.01 ± 0.11	24 ± 6	–	–
70	127	15.41	3.04 ± 0.06	10 ± 2	3.42 ± 0.06	18 ± 2	3.32 ± 0.03	11 ± 2	–	–
71	130	14.83	1.11 ± 0.13	23 ± 6	1.21 ± 0.07	32 ± 2	1.25 ± 0.23	28 ± 8	–	–
72	129	14.66	3.96 ± 0.27	15 ± 2	4.20 ± 0.36	14 ± 2	3.76 ± 0.06	17 ± 2	–	–
73	95	14.38	1.32 ± 0.13	33 ± 3	1.45 ± 0.08	35 ± 2	1.37 ± 0.05	31 ± 2	0.75	–
74	93	12.08	2.69 ± 0.01	6 ± 2	2.74 ± 0.04	4 ± 2	2.52 ± 0.09	2 ± 2	0.97	0.81
75	94	14.50	2.82 ± 0.55	10 ± 6	3.16 ± 0.44	17 ± 4	2.79 ± 0.12	9 ± 2	–	–
76	91	12.27	3.01 ± 0.03	11 ± 2	3.23 ± 0.08	12 ± 2	3.06 ± 0.10	13 ± 2	0.95	–
77	–	15.33	1.27 ± 0.08	166 ± 2	1.26 ± 0.09	165 ± 3	1.18 ± 0.14	161 ± 5	–	–
78	–	15.78	1.50 ± 0.29	22 ± 3	1.66 ± 0.23	24 ± 3	1.43 ± 0.08	16 ± 2	–	–
79	–	16.19	1.96 ± 0.19	5 ± 3	2.31 ± 0.24	10 ± 3	2.02 ± 0.39	8 ± 5	–	–
80	–	16.3	3.23 ± 0.22	21 ± 2	3.37 ± 0.40	24 ± 4	3.46 ± 0.35	29 ± 6	–	0.89
81	128	16.26	4.02 ± 0.29	6 ± 6	4.12 ± 0.28	8 ± 5	4.15 ± 0.12	9 ± 3	–	–
82	–	14.54	0.89 ± 0.22	7 ± 4	1.01 ± 0.20	8 ± 3	0.85 ± 0.21	4 ± 4	–	0.46
83	–	14.35	1.29 ± 0.12	21 ± 3	1.51 ± 0.11	25 ± 2	1.15 ± 0.19	19 ± 3	–	–
84	–	14.29	1.16 ± 0.09	12 ± 3	1.21 ± 0.16	18 ± 6	1.07 ± 0.14	10 ± 5	–	–
85	–	11.78	0.73 ± 0.02	24 ± 3	0.76 ± 0.03	21 ± 2	0.77 ± 0.05	27 ± 3	–	–
86	–	15.99	2.63 ± 0.50	110 ± 7	2.78 ± 0.58	113 ± 8	2.79 ± 0.62	116 ± 8	–	–
87	–	15.44	3.58 ± 0.21	20 ± 2	3.67 ± 0.10	27 ± 2	3.48 ± 0.06	25 ± 2	–	–
88	–	13.86	2.35 ± 0.28	30 ± 4	2.46 ± 0.11	39 ± 2	2.34 ± 0.12	33 ± 2	–	–
89	–	15.64	3.11 ± 0.32	12 ± 6	3.41 ± 0.28	15 ± 4	3.26 ± 0.43	18 ± 8	–	–
90	–	15.81	4.17 ± 0.68	30 ± 6	4.23 ± 0.35	37 ± 2	4.26 ± 0.12	37 ± 2	–	–
91	–	16.21	3.18 ± 0.27	21 ± 3	3.24 ± 0.12	24 ± 2	3.16 ± 0.48	20 ± 5	–	–
92	184	13.82	3.21 ± 0.11	24 ± 2	3.16 ± 0.21	21 ± 2	3.17 ± 0.28	24 ± 2	–	–
93	179	13.12	1.85 ± 0.20	17 ± 3	2.05 ± 0.17	21 ± 2	1.87 ± 0.05	19 ± 2	0.97	0.89
94	180	12.5	2.49 ± 0.02	15 ± 2	2.75 ± 0.17	16 ± 2	2.41 ± 0.02	16 ± 2	–	0.00
95	–	15.05	2.45 ± 0.44	27 ± 5	2.60 ± 0.29	25 ± 3	2.35 ± 0.20	21 ± 3	–	–
96	191	14.3	2.54 ± 0.21	19 ± 3	2.87 ± 0.44	18 ± 8	2.48 ± 0.27	22 ± 3	–	–
97	–	14.38	2.17 ± 0.59	18 ± 8	2.27 ± 0.09	25 ± 2	2.27 ± 0.39	28 ± 5	–	–
98	185	14.48	2.78 ± 0.29	18 ± 4	2.89 ± 0.26	23 ± 2	2.69 ± 0.31	18 ± 3	–	0.88
99	22	14.88	2.20 ± 0.43	36 ± 6	2.27 ± 0.36	38 ± 5	2.16 ± 0.11	37 ± 4	–	0.07
100	186	14.67	3.51 ± 0.17	10 ± 2	3.77 ± 0.03	13 ± 2	3.60 ± 0.16	13 ± 2	–	0.57
101	192	14.96	2.73 ± 0.10	35 ± 2	3.04 ± 0.37	27 ± 3	2.55 ± 0.23	21 ± 3	–	0.47
102	187	14.37	2.97 ± 0.05	20 ± 2	3.29 ± 0.02	18 ± 2	2.75 ± 0.10	20 ± 2	–	0.81
103	–	14.63	4.11 ± 0.93	13 ± 2	4.20 ± 0.46	15 ± 3	3.95 ± 0.52	15 ± 4	–	0.89
104	29	15.33	4.30 ± 0.06	11 ± 2	4.33 ± 0.06	12 ± 2	4.35 ± 0.25	10 ± 2	–	0.24

†According to this observation.
††According to Barkhatova (1957).
*According to Erickson (1971).
**According to Dias et al. (2006).

where F_o and F_e represent the effects mentioned above and the ratio is given by

$$\frac{F_o}{F_e} = \left[\frac{I'_o(0°)}{I'_e(45°)} \times \frac{I'_o(45°)}{I'_e(0°)} \times \frac{I'_o(22.5°)}{I'_e(67.5°)} \times \frac{I'_o(67.5°)}{I'_e(22.5°)} \right]^{1/4}. \quad (4)$$

Substituting the ratio in equation (3) and fitting the cosine curve to the four values of $R(\alpha)$, the values of P and θ can be obtained. The individual errors associated with the four values of $R(\alpha)$ are used as a weight while calculating P, θ and their respective errors.

Four polarimetric standard stars and four secondary polarimetric standard stars for null polarization and for the zero-point of the polarization position angle were taken from Schmidt, Elston & Lupie (1992) and Turnshek et al. (1990) respectively. The observed degrees of polarization as a percentage ($P\%$) and position angles in degrees ($\theta°$) for the polarized standard stars and their corresponding values from Schmidt et al. (1992) and Turnshek et al. (1990) are given in Table 1. The observed values of $P\%$ and $\theta°$ are in good agreement with those given in Schmidt et al. (1992) and Turnshek et al. (1990), within the observational errors. The observed normalized Stokes parameters q and u in percentage ($q\%$, $u\%$) for standard unpolarized stars are also given in Table 1. The average value of instrumental polarization is found to be less than 0.05 per cent in all passbands. The instrumental polarization of AIMPOL on the 104-cm Sampurnanand Telescope has been monitored since 2004 in different projects and found to be nearly invariant in

Table 3. Results of previous polarization measurements carried out by Serkowski (1965) in the direction of NGC 6823.

ID(B) (1)	$P_B \pm \epsilon$(per cent) (2)	θ_B (3)	$P_V \pm \epsilon$(per cent) (4)	θ_V (5)	M_P (6)
Serkowski (1965)					
3	4.14 ± 0.23	06	4.19 ± 0.23	06	0.97
9	4.51 ± 0.32	172	4.84 ± 0.32	175	0.97
11	5.11 ± 0.46	05	4.47 ± 0.46	04	0.97
13	2.95 ± 0.14	11	3.32 ± 0.14	09	0.95
17	2.81 ± 0.51	13	3.36 ± 0.51	16	0.97
54	–	–	0.83 ± 0.28	03	–
68	4.38 ± 0.46	14	5.34 ± 0.46	12	0.96
73	–	–	0.23 ± 0.18	30	–
74	2.58 ± 0.46	13	3.64 ± 0.46	12	0.97
78	3.41 ± 0.55	02	4.10 ± 0.55	09	0.93
189	–	–	0.23 ± 0.14	52	–
BD +23° 3745	6.40 ± 0.14	27	6.63 ± 0.14	24	0.88

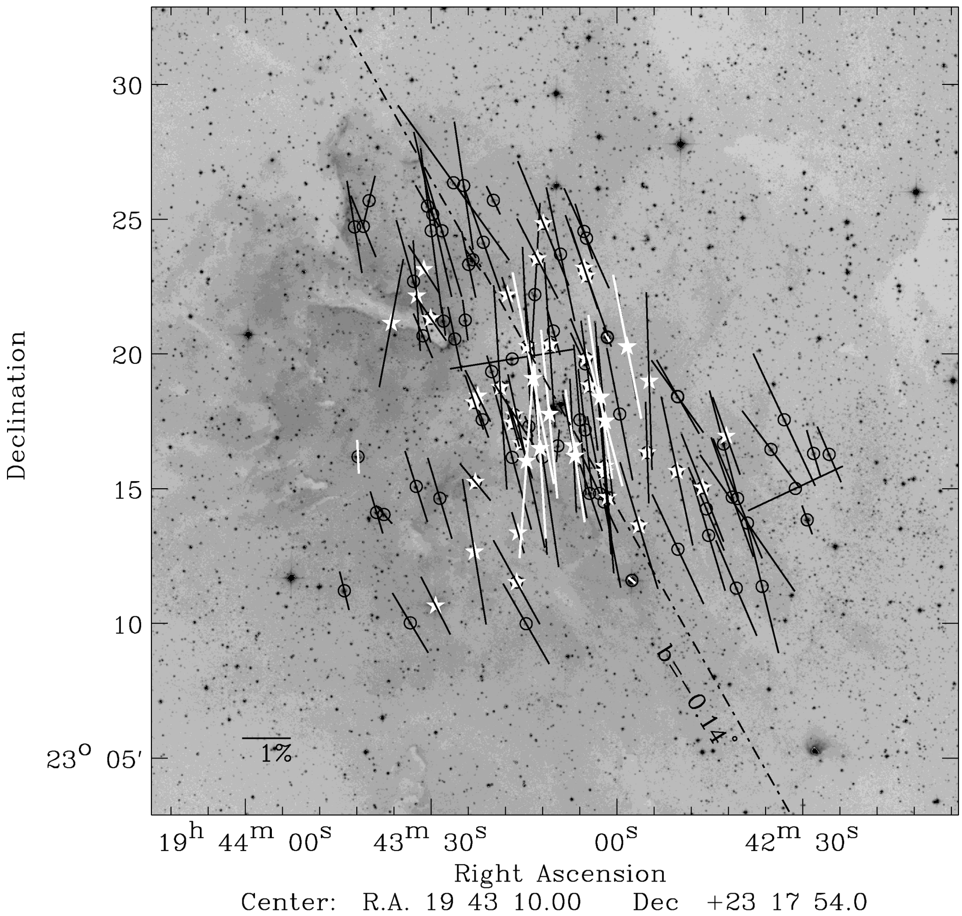

Figure 1. The 30 × 30 arcmin^2 R-band DSS2 image of the field containing NGC 6823, reproduced from Digitized Sky Survey II. The position angles, in the equatorial coordinate system, are measured from the north, increasing eastward. The polarization vectors are drawn with the star as the centre. The length of the polarization vectors is proportional to the percentage of polarization P_V, and is oriented parallel to the direction corresponding to the observed polarization position angle θ_V. A vector with a P of 1 per cent is shown for reference. The dashed line represents the Galactic parallel at $b = -0\overset{\circ}{.}14$. Stars with $M_{\rm P} \geq 0.50$ are identified with filled star symbols in white. Polarization vectors of 12 stars observed by Serkowski et al. (1965) are shown in white.

different passbands (Rautela, Joshi & Pandey 2004; Medhi et al. 2007, 2008; Pandey et al. 2009).

AIMPOL has no grid placed to avoid the overlapping of the ordinary image of one source with the extraordinary image of an adjacent one located 27 pixels away along the north–south direction. We therefore avoided the central crowded portion of the cluster. However, the fields are chosen in such a manner as to include the maximum number of member stars. We also had a large number of

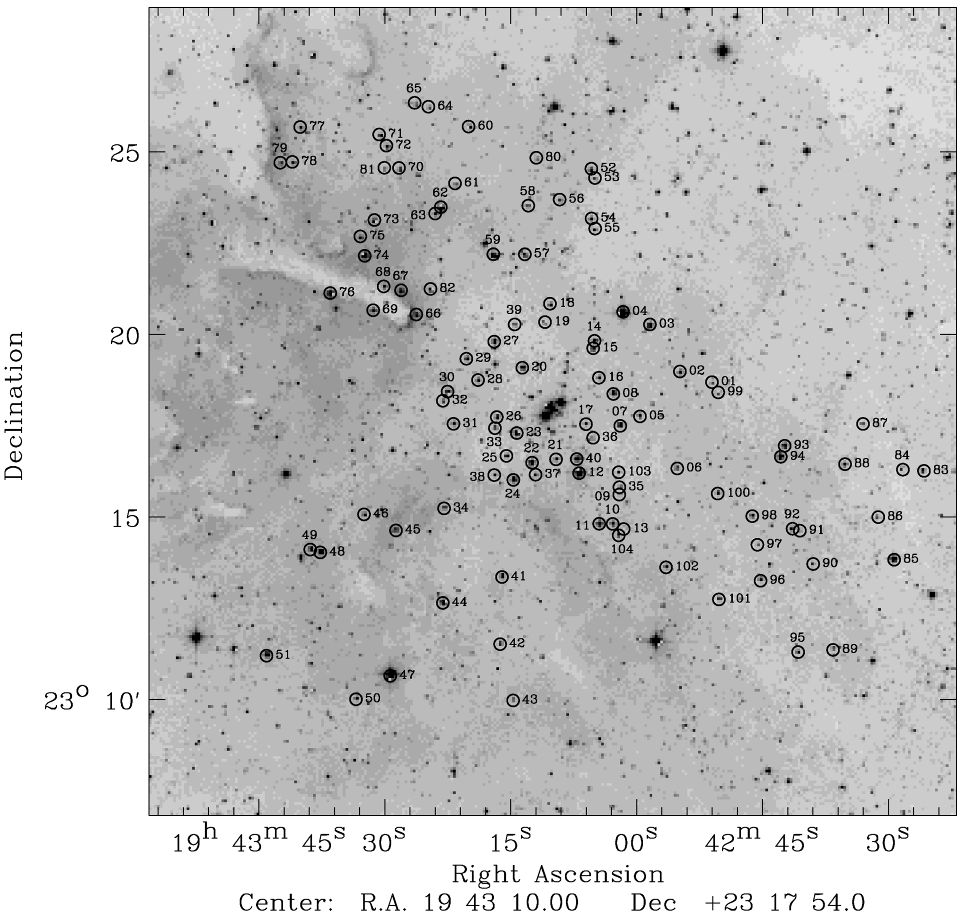

Figure 2. The 25 × 25 arcmin^2 *R*-band DSS2 image of the field containing NGC 6823, reproduced from Digitized Sky Survey II. The field is identified according to the star identification number ID(M).

sources that are not members but are present in the fields observed. All the sources were manually checked and rejected in cases of an overlapping image.

3 RESULTS AND DISCUSSION

The results of our polarimetric observations towards NGC 6823 are presented in Table 2. The star identification numbers ID(M) and ID(B) are given in columns 1 and 2, following this observation and Barkhatova (1957) respectively. The instrumental magnitudes obtained in the *V* filter are given in column 3. The measured values of polarization $P\%$ and corresponding error $\epsilon\%$ in *B*, *V* and R_c filters are given in columns 4, 6 and 8, respectively. The polarization position angle (of the *E* vector) θ° and the corresponding error ϵ° in *B*, *V* and R_c filters are given in columns 5, 7 and 9, respectively. The position angles in the equatorial coordinate system are measured from the north, increasing eastward. Columns 10 and 11 represent the membership probabilities $M_{\rm P}$(E) and $M_{\rm P}$(D) according to Erickson (1971) and Dias et al. (2006), respectively. Stars with $M_{\rm P} \geq 0.50$ are considered as cluster members in this study.

The previous polarimetric measurements of stars in the direction of NGC 6823 carried out by Serkowski (1965) are presented in Table 3. Serkowski (1965) observed 22 stars in the direction of NGC 6823 using *B* and *V* photometric bands. Out of 22 stars observed by Serkowski (1965), we have included only 12 stars in our study, which have RA and Dec. available. In column 1 we give the identification numbers, which are adopted from Barkhatova (1957). $P\%$ and θ° in the *B* and *V* filters are given in columns 2, 3, 4 and 5, respectively. We converted *p* to $P\%$ using the relation $P\% = 46.05p$ (Whittet 1992). In column 6 we give the membership probabilities of stars obtained from Erickson (1971).

Fig. 1 presents the sky projection of the *V*-band polarization vectors for the 104 stars observed by us in NGC 6823 (the *R*-band image is reproduced from the Digitized Sky Survey II). The finding chart of the stars are shown in Fig. 2. The polarization vectors are drawn at the centre of the observed stars. The length of the polarization vector is proportional to the percentage of polarization in the *V* band (P_V) and the vector is oriented parallel to the direction of the corresponding observed polarization position angle in degrees in the *V* band (θ_V). The dashed line represents the Galactic parallel at $b = -0\overset{\circ}{.}14$, inclined at $\sim 32^\circ$ with respect to the north. The stars with $M_{\rm P} \geq 0.50$ are identified using closed star symbols in white. Polarization vectors for 12 stars observed by Serkowski (1965) are shown in white.

In Fig. 3, we present the sky projection of the *B*-band polarization vectors for the 104 stars observed by us towards NGC 6823 (vectors in black), along with the results from Serkowski (1965) (vectors in white), and in Fig. 4 we present only the sky projection of the R_c-band polarization vectors for the 104 stars observed by us in NGC 6823 (vectors in black), because there are no observations by Serkowski (1965) in the *R* filter.

There are eight stars in common between Serkowski (1965) and the present observations. The polarization and position angles for

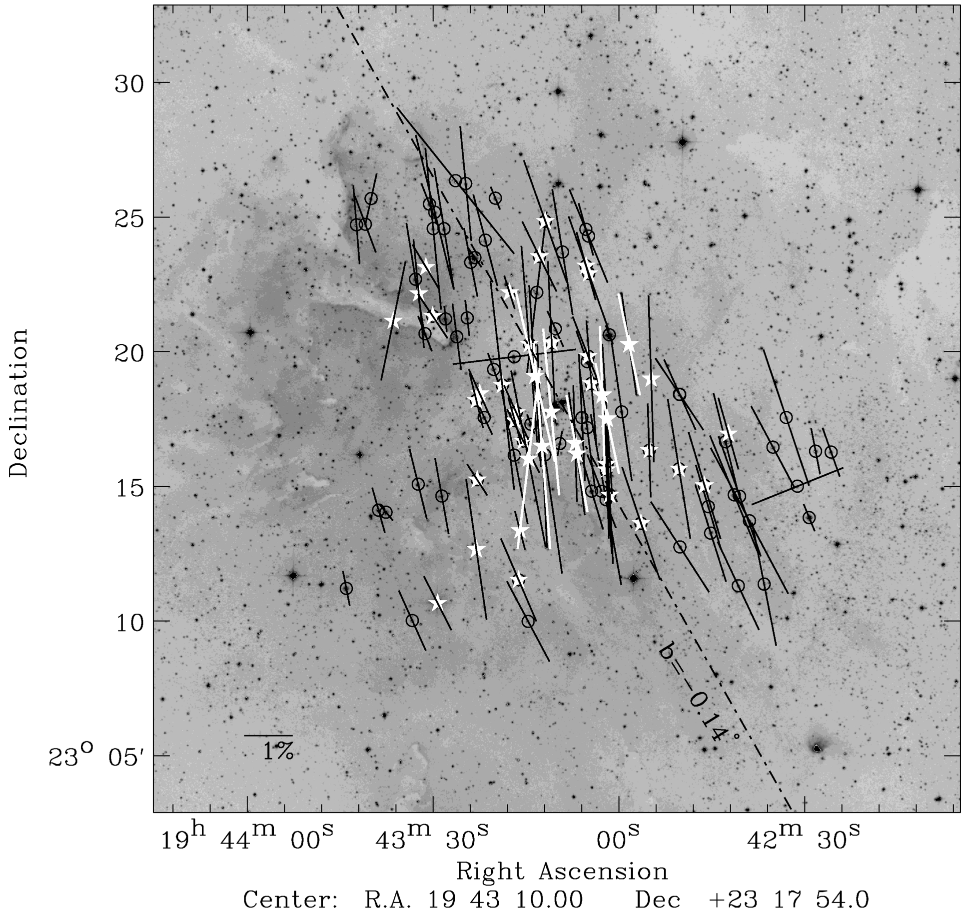

Figure 3. As Fig. 1, but for P_B and θ_B. Results for 9 stars observed by Serkowski (1965) using the B filter are shown using vectors drawn in white.

the eight common stars in the B and V filters seem to be consistent within the uncertainty in both observations. From the sky projection of the polarization vectors for the 104 stars observed by us in all three filters, it is clear that the polarization vectors of the stars are distributed about the Galactic plane and lower than the Galactic plane (especially for those located at the centre of the cluster).

Fig. 5 shows the distribution of the polarization and position angles in the V filter (P_V and θ_V) for the 42 member stars with a radial distance from the cluster centre. We have chosen RA(J2000) $19^{\mathrm{h}}43^{\mathrm{m}}09^{\mathrm{s}}$, Dec.(J2000) + $23°18^{\mathrm{m}}00^{\mathrm{s}}$ as the centre of the cluster, taken from Kharchenko et al. (2005) who use the approximation of the maximum surface density of cluster members for locating the cluster centre. The upper and lower left-hand panels of Fig. 5 show the distribution of position angle and polarization in the V filter with radial distance from the cluster centre. The position angles are found to show a systematic change, while the polarization is found to reduce towards the outer parts of the cluster. In both plots it is noticeable that the member stars preferentially follow two separate distributions, which are shown by the histograms in the upper and lower right-hand panels of Fig. 5. From the cluster centre to a radial distance of 4 arcmin, the stars show a trend of lower position angle and higher polarization (black asterisks) than the stars lying at a radial distance of above 4 arcmin (black filled circles). Stone (1988) also found a boundary at $r \simeq 3.5$ arcmin, and he defines the region from the cluster centre to $r \simeq 3.5$ arcmin as the nucleus and above $r \simeq 3.5$ arcmin as the coronal region of the cluster NGC 6823. Other authors like Barkhatova (1957) found the radius for the nuclear region as $r \simeq 4.0$ arcmin, while Turner (1979) quote it as $r \simeq 2.5$ arcmin. In general, every cluster consists of two main regions, a nucleus and a corona. The nucleus is the densest, central part of the cluster, which is perceived directly by our eye as a cluster. The corona is the outer, extended, less dense region around the cluster. For many distant clusters, the coronae are lost against the rich star field.

The right-hand upper and lower panels of Fig. 5 present the distribution of the 42 member stars belonging to the nucleus and the coronal region shown by the dashed and solid histograms. In NGC 6823, out of 42 member stars 24 stars belong to the nucleus and 18 stars belong to the coronal region. Two significantly different distributions of the polarization and position angle are followed by the stars belonging to the nucleus and the coronal region, as shown in the histograms in Fig. 5. The weighted mean values of polarization (P_V) and position angle (θ_V) in the V filter are 3.66 ± 0.02 per cent, $8° \pm 1$ for the nucleus and 3.10 ± 0.02 per cent, $25° \pm 1$ for the coronal region, respectively. The average value of the position angle of the coronal region is closer to the inclination of the Galactic parallel ($\sim 32°$) than that for the nuclear region. The distribution of polarization vectors about the Galactic plane indicates that the dust grains present in the coronal region are mostly aligned by a magnetic field that is nearly parallel to the direction of the Galactic disc. In the nucleus the distribution of polarization vectors lower than the Galactic plane suggests that a second component of magnetic field, slightly less inclined to the Galactic disc, could also be present.

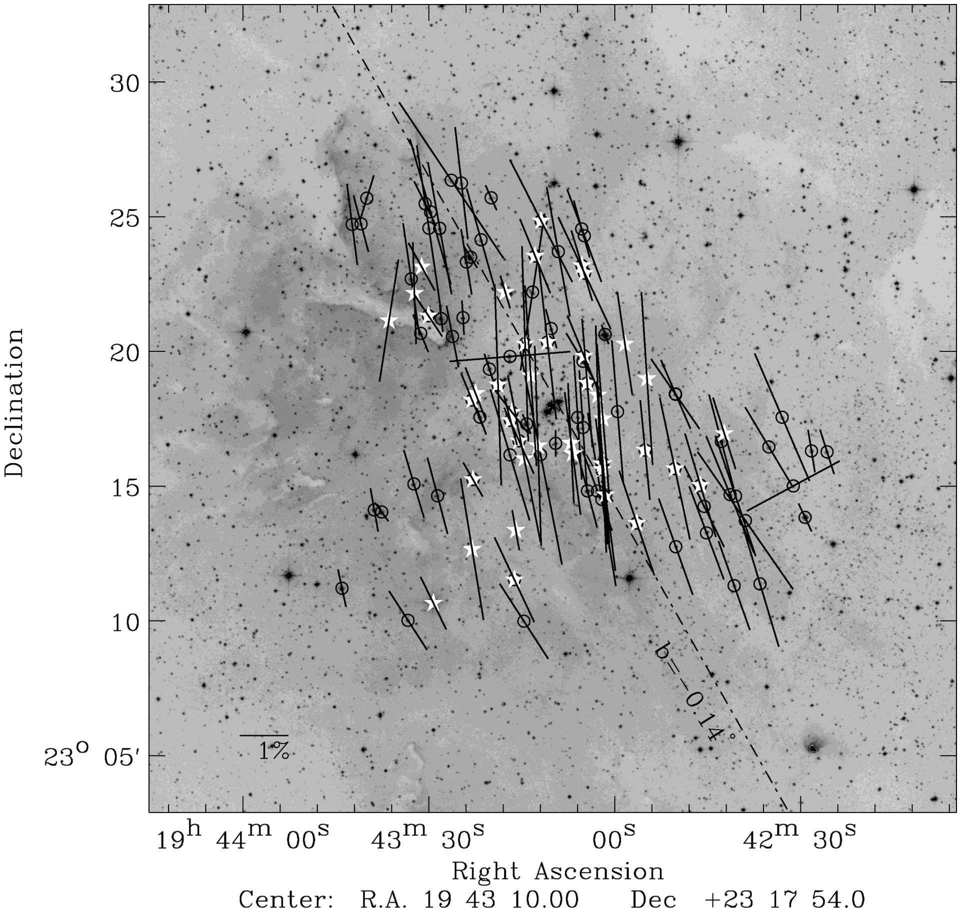

Figure 4. As Fig. 1, but for P_R and θ_R.

In the radial distribution plots (Fig. 5), it can also be seen that the polarization (P_V) data points are more scattered in the nucleus compared with the coronal region, while the position angle (θ_V) data points show the same behaviour (highly scattered) in both regions. The highly scattered P_V data points in the nuclear region indicate that the density of intracluster dust/materials may be higher and its distribution more differential than for the coronal region. The presence of different generations of dust particles and different components of the local magnetic field may be the cause for the highly scattered θ_V data points in the radial plot for both regions.

To check the consistency of our results, we use the Heiles (2000) catalogue, which has a compilation of over 9000 polarization measurements. We found 19 stars with polarization measurements in the V band, within a circular region of radius $\simeq 2^\circ$ around NGC 6823. Fig. 6 presents a P_V versus θ_V plot. Our results are represented by open squares. The polarizations and position angles in the visual filter taken from Heiles (2000) are represented by filled black circles. The stars with $M_{\rm P} \geq 0.50$ are identified using asterisks. The stars from Heiles (2000) show a degree of polarization ($P_{\rm H}$) in the range $\sim$0.01–6.36 per cent. The mean value of $P_{\rm H}$ and position angle ($\theta_{\rm H}$) are $\simeq 2.21 \pm 0.86$ per cent and $\simeq 28 \pm 10^\circ$, respectively. In our observation, the P_V of the stars is found to be in the range $\sim$0.52–5.50 per cent. The stars cluster towards lower position angle. The mean values of P_V and θ_V are found to be $\sim 2.58 \pm 0.39$ per cent and $\sim 26 \pm 4^\circ$, respectively.

The mean values of polarization and position angle for a smaller region of $\sim 25 \times 25$ arcmin^2 centring on NGC 6823 obtained by us are quite similar to those for a larger region from Heiles (2000). The polarization must therefore likely be due to the contribution from dust grains distributed in an extended structure closer to us, and the small intracluster contribution. Consequently, knowledge about the distribution of interstellar dust towards the direction of NGC 6823 is very important, in order to interpret our polarimetric results.

3.1 Distribution of interstellar matter in the region of NGC 6823

The colour excess $E(B-V)$ of this cluster for main-sequence stars varies from 0.60–1.16 mag (Sagar & Joshi 1981; Sagar 1987). Moreover, a relatively larger value of colour excess is found at the centre and along the diagonal joining the north-west and south-east corners of the cluster (Sagar & Joshi 1981). In NGC 6823, there is a slight tendency for the $E(B-V)$ of the stars in the eastern part of the cluster to exhibit a large value of R_V. The cluster NGC 6823 is surrounded by a reflection nebula, NGC 6820. The extinction is highest at the eastern part of the cluster as this is the direction of the reflection nebula. However, excluding supergiants the reddening law for the whole cluster can be characterized by $R_V = 3.2 \pm 0.1$ (Guetter 1992).

By using the 'Digitized Sky Survey I' optical data base and applying a traditional star-count technique, Dobashi et al. (2005) produced extinction maps of the entire region of the Galaxy in the Galactic latitude range $|b| \leq 40^\circ$. We have used their fits of the extinction map of the field containing NGC 6823, available online.[1]

[1] http://darkclouds.u-gakugei.ac.jp/astronomer/astronomer.html

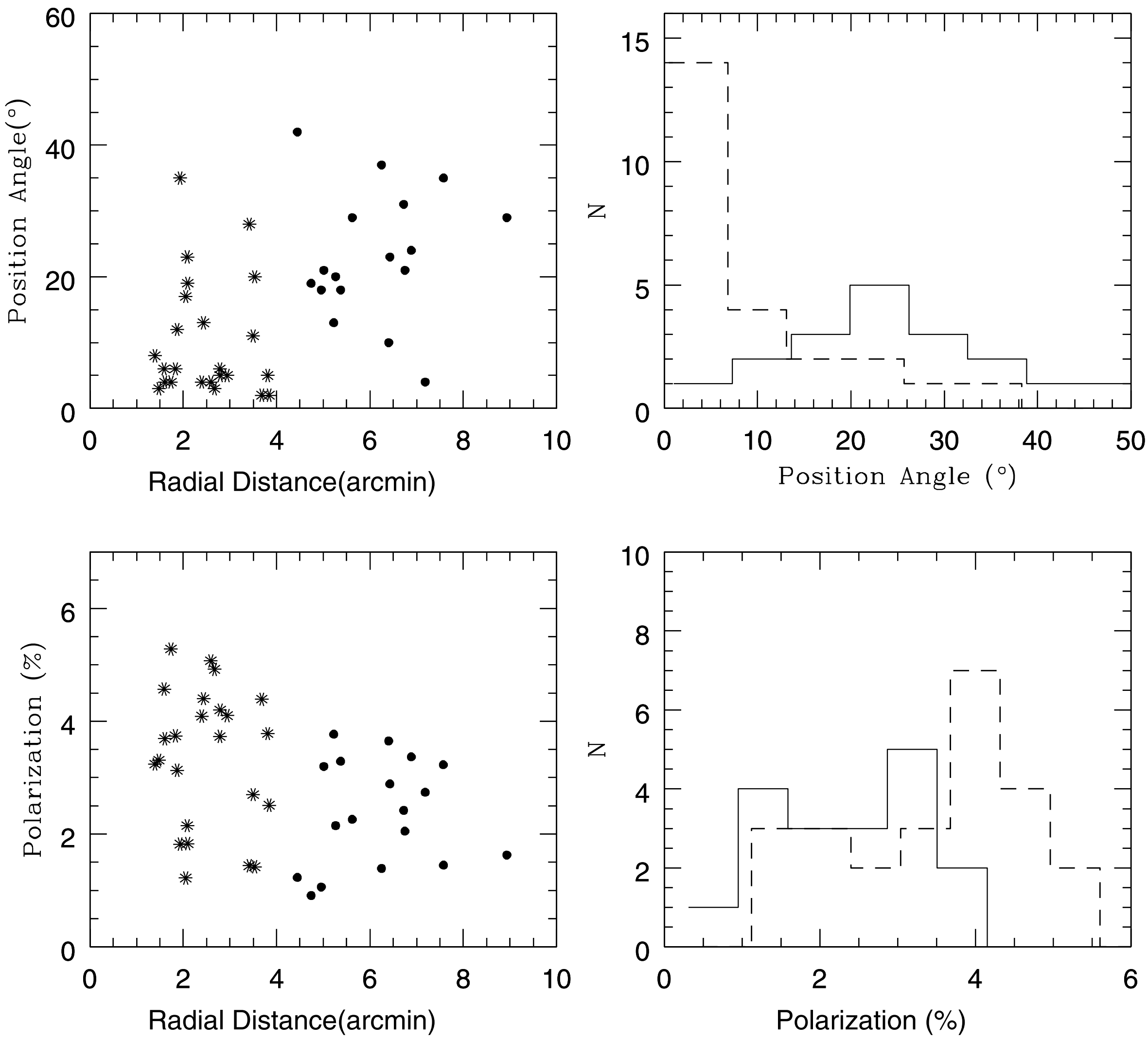

Figure 5. The distribution of P_V and PA_V for 42 member stars, with their radial distance from the cluster centre.

The high-resolution extinction map, overlaid with V-band results from our observations, is shown in Fig. 7. We transformed all position angles measured relative to the equatorial north to the Galactic north using the relation given by Corradi, Aznar & Mampaso (1998), because the A_V maps are in Galactic coordinates. The black circle identifies the centre of the cluster ($l = 59\overset{\circ}{.}40$, $b = -0\overset{\circ}{.}144$). The greyscale colour bar on the right-hand side of the extinction map shows the range of A_V values in the figure. The contours are plotted at $A_V = 0.5$–4 with an interval of 0.5 mag.

The extinction towards the location of the cluster (black circle) shows relatively low ($A_V \sim 3$) values. However, in the outer regions of the cluster, especially towards the south and the east, the extinction increases up to ∼4 mag. One clump identified by Dobashi et al. (2005) in this region is labelled as P10 in Fig. 7. There is only one dark cloud, LDN 791, identified by Lynds (1962), located radially 40 arcmin away from the clump P10 in a south-easterly direction. The value of extinction estimated by previous observers (Guetter 1992; Feinstein 1994; Sagar & Joshi 1981) towards the centre of the cluster is in close agreement with Dobashi et al. (2005).

The Columbia 1.2-m millimetre-wave telescope CO emission survey of NGC 6823 by Leisawitz, Bash & Thaddeus (1989) identifies five molecular clouds around it at the cluster distance. The velocities and masses of the clouds range from 23.7 km s^{-1} to 34.8 km s^{-1} and 11×10^3 M$_\odot$ to 110×10^3 M$_\odot$, respectively. The Balloon-borne Large Aperture Submillimetre Telescope (BLAST) also detects 60 compact submillimetre sources simultaneously at 250, 350 and 500 μm (Chapin et al. 2008) towards NGC 6823. Of these 60 compact submillimetre sources, 49 of them are found to be associated with NGC 6823.

To get an idea of the distances to the foreground dust concentration, it is very important to study the distribution of polarization at different distances along that particular line of sight. To investigate the polarization properties/distribution of dust grains towards NGC 6823 located at different distances, we therefore selected all the stars from Heiles (2000) within a circle of radius 5° around NGC 6823 with available polarization data ($P_{\rm H}$). The parallax measurements for the stars are obtained from the *Hipparcos* and Tycho catalogues (Perryman et al. 1997; Høg et al. (1997). Applying a 2σ rejection limit criterion to the parallax, we found parallax measurements available only for 45 stars, covering maximum distances up to 800 pc. Stars that showed peculiar features and emissions in their spectrum, as given by SIMBAD, are rejected.

Fig. 8 presents the degree of polarization ($P_{\rm H}$) versus distance plot. The stars located closer to us show lower values of

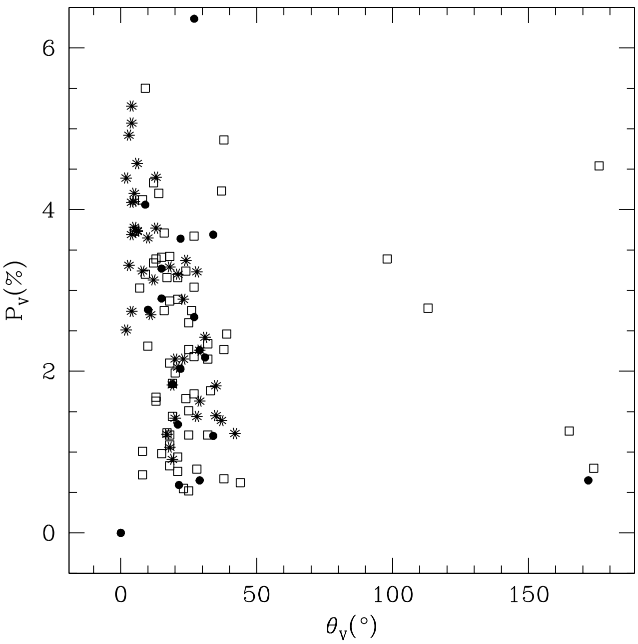

Figure 6. P_V versus θ_V plot for 104 stars observed by us in the direction of NGC 6823, shown using open squares. Stars taken from Heiles (2000) are shown by filled black circles. The stars with $M_P \geq 0.50$ are identified using asterisks.

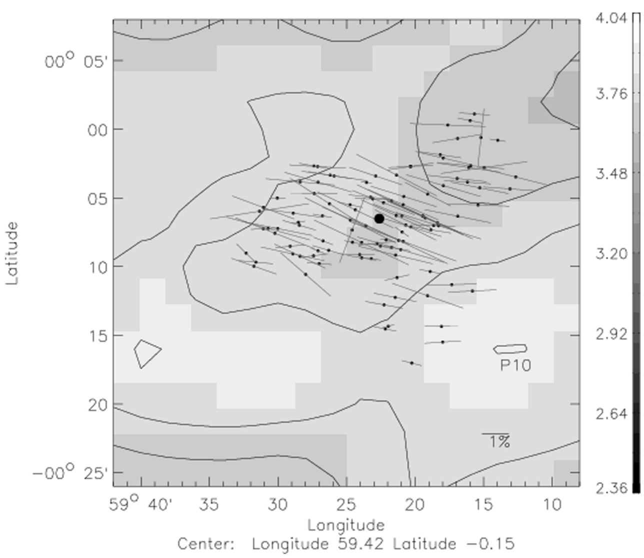

Figure 7. The high-resolution extinction map of the region (30 × 30 arcmin^2) produced by Dobashi et al. (2005) using the optical data base ‘Digitized Sky Survey I’ and applying a traditional star-count technique. We overlay V-band results from our observations using vectors drawn in black. The clump identified by Dobashi et al. (2005) in this region is identified and labelled as P10. The centre of the cluster ($l = 59\overset{\circ}{.}40$, $b = -0\overset{\circ}{.}14$) is identified using a black circle.

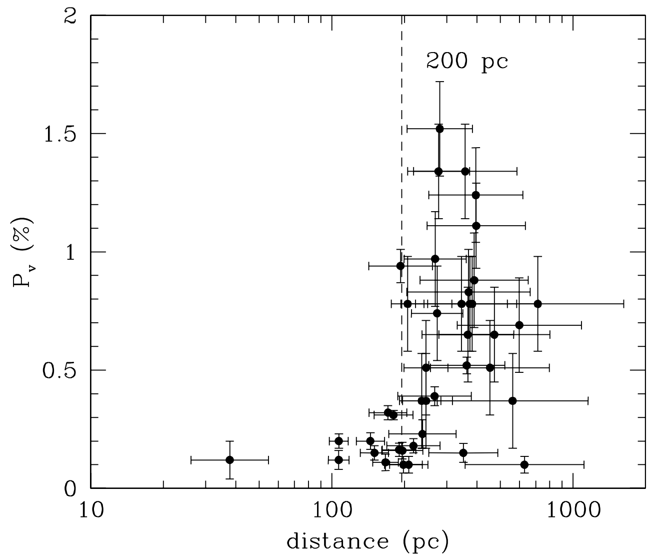

Figure 8. Distance versus P_V% plot, using data obtained from Heiles (2000) and Perryman et al. (1997). The dotted line is drawn at 200 pc to show a sharp increase in the P_V % value at this distance.

P_H ($\lesssim$0.2 per cent) than the stars located beyond ~200 pc, which show relatively high values of P_H in the range from 0.2–1.5 per cent, with a sharp jump in polarization occurring at ~200 pc. Only one star is available in the range ~10–100 pc, so from Fig. 8 we can infer only a maximum distance of 200 pc to the dust grains responsible for the observed sharp jump and assign a maximum distance of 200 pc to the first layer of dust towards NGC 6823.

Since most of the extinction/reddening is produced by the foreground interstellar material, it is necessary to investigate the evolution of the interstellar environments from the Sun to the cluster. In Fig. 9, we have plotted the Stokes parameters $Q_V(= P_V \cos 2\theta_V)$ and $U_V(= P_V \sin 2\theta_V)$ in the V filter, for each of the 42 observed member stars. In the figure, the coordinates $Q_V = 0$ and $U_V = 0$ represent the dustless solar neighbourhood. The points lying on other parts of the figure indicate the direction of the polarization vector as seen from the Sun. The member stars over this region roughly segregate into three different polarimetric groups according to their distribution in the Stokes plane. The solid lines in Fig. 9 represent the changing direction of the vector P_V, connecting the weighted mean values of Q_V and U_V for the three possible different groups. The nearby group consists of 10 member stars (namely #5, #33, #35, #62, #63, #65a, #82, #95, #68M and #34M; identification number suffix ‘M’ denotes identification according to ID(M), otherwise ID(B) is used), with a weighted mean value of polarization 1.34 ± 0.04 per cent and position angle 33 ± 1°. This nearby group lies almost parallel to the Galactic plane. The next group has six member stars (namely #8, #36, #75, #80, #179 and #58M) with weighted mean value of polarization and position angle 1.93 ± 0.05 per cent and 23 ± 1°, respectively. The remaining 26 member stars (namely #9, #11, #13, #14, #17, #20, #23, #25, #28, #34, #65, #68, #70, #74, #76, #78, #79, #91, #93, #185, #186, #187, #9M, #39M, #80M and #103M) are in the third group, which has a weighted mean value of polarization 3.64 ± 0.01 per cent and position angle 11 ± 1°.

The evolution of polarization towards NGC 6823 is likely to be due to the patchy distribution of dust, and the core may be behind a low, dense layer of dust or a hole. Some of the authors who made photometric studies of NGC 6823 believe that towards this cluster the distribution of dust is patchy, e.g. Guetter (1992) indicates that the reddening towards this cluster may be constant in small spatial areas but is highly variable across the face of the cluster and ranges from 1.07–0.64 mag. This absorption variability has also been noticed by many earlier investigators and can easily be seen by examining the colour–magnitude and colour–colour plots as published by Hoag et al. (1961).

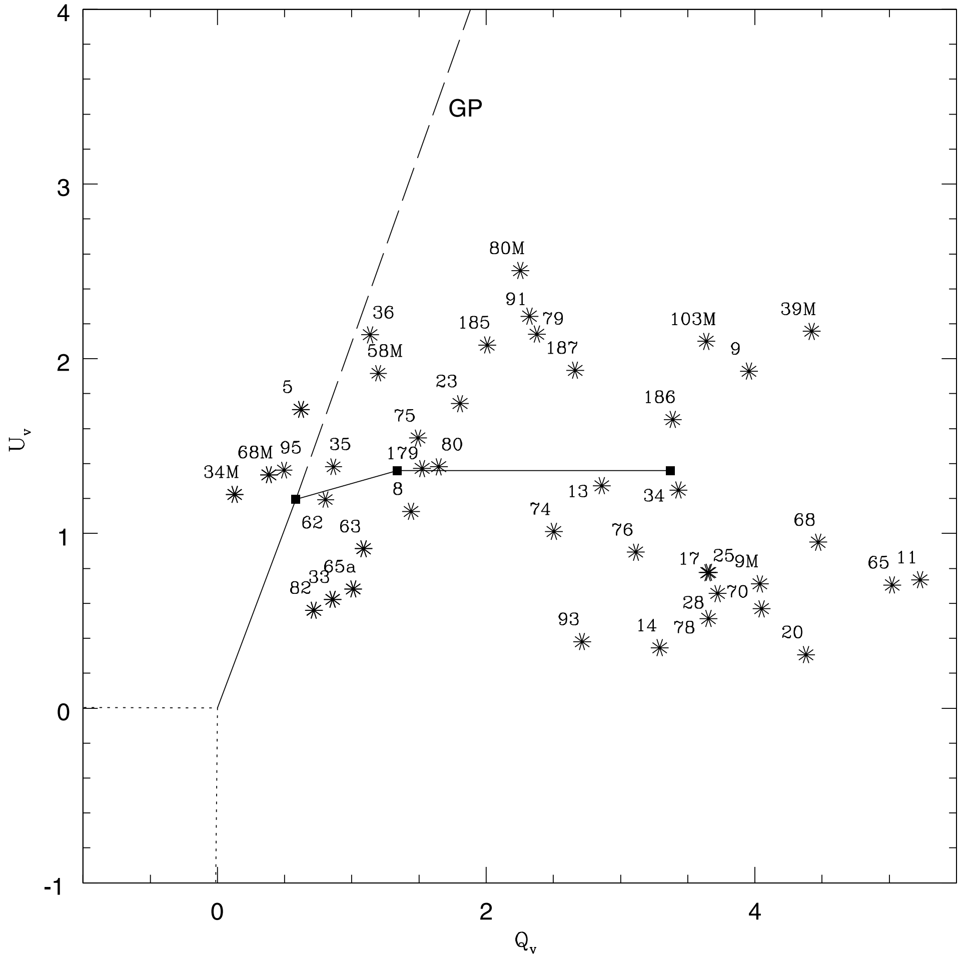

Figure 9. The U_V versus Q_V plot for 42 member stars observed by us in the direction of NGC 6823. The dashed line is in the direction of the Galactic plane (GP). The solid line is the interpretation of the evolution of polarization through the dust layer between the cluster and the Sun.

From the optical photometric study, Neckel & Klare (1980) found that more than half of the total extinction towards the cluster NGC 6823 comes from matter lying close to us, at a distance in range 0.2–0.5 kpc. The presence of nearby interstellar matter at a distance of $\sim$300 pc in the direction of the cluster was also recently confirmed by Fresneau & Monier (1999). They noticed a systematic absorption of about 1.5 mag in the V band in this region. The absorbing matter in this region is probably located at the depth of the Vulpecula rift molecular cloud (Dame & Thaddeus 1985). Therefore, we believe that the observed polarization towards NGC 6823 is mainly due to layers of nearby aligned dust grains of patchy structure associated with the above-mentioned clouds.

3.2 Serkowski law

The maximum wavelength ($\lambda_{\max}$) and the maximum polarization ($P_{\max}$) are both functions of the optical properties and the characteristics of particle size distribution of the aligned dust grains (McMillan 1978; Wilking et al. 1980). Moreover, they are also related to the interstellar extinction law (Serkowski et al. 1975; Whittet & van Breda 1978; Coyne & Magalhaes 1979; Clayton & Cardelli 1988). The values of $\lambda_{\max}$ and $P_{\max}$ have been calculated by fitting the observed polarization in the B, V and R_c bandpasses to the standard Serkowski's polarization law:

$$P_\lambda / P_{\max} = \exp\left[-k \ln^2(\lambda_{\max}/\lambda)\right], \tag{5}$$

adopting the parameter $k = 1.15$ (Serkowski 1973). In the fits a degree of freedom of 1 is adopted. Although there are only three data points, the wavelength covered ranges from 0.44–0.66 μm and all the $\lambda_{\max}$ are found to fall within this range. Since we have enough wavelength coverage, the fit is reasonably good, but sometimes it overestimates the value of σ_1. For each star we computed the σ_1 parameter (the unit weighting error of the fit). If the polarization is well represented by Serkowski's interstellar polarization law, σ_1 should not be higher than 1.6, due to the weighting scheme. A higher value could be indicative of the presence of intrinsic polarization. The $\lambda_{\max}$ values can also give us a clue as to the origin of polarization. Stars that have $\lambda_{\max}$ lower than the average value for the interstellar medium (0.55 ± 0.04 μm, Serkowski et al. 1975) are probable candidates for having an intrinsic component of polarization (Orsatti, Vega & Marraco 1998). The dispersion of the position angle ($\overline{\epsilon}$) for each star normalized by the mean value of the position-angle error is another tool with which to detect intrinsic polarization. The values obtained for $P_{\max}$, $\lambda_{\max}$, σ_1 and $\overline{\epsilon}$, together with ID(M), ID(B), RA(2000J) and Dec.(2000J) for all 104 observed stars, with their respective errors, are given in Table 4. Column 9 in Table 4 represents $E(B-V)$, available only for 21 member stars and five non-member stars. In that table the values of $E(B-V)$ suffixed by (G), (S) and (E) are taken from Guetter (1992), Stone (1988) and Erickson (1971), respectively.

Table 4. Values of $P_{\max}$, $\lambda_{\max}$, σ_1 and $\overline{\epsilon}$ for the observed data in NGC 6823.

ID(M)† (1)	ID(B)†† (2)	RA(2000J) (3)	Dec.(2000J) (4)	$P_{\max} \pm \epsilon$ (per cent) (5)	$\lambda_{\max} \pm \epsilon$ (μm) (6)	σ_1 (7)	$\overline{\epsilon}$ (8)	$E(B-V)$ (9)
01	–	19 42 51.00	23 18 42.2	2.08 ± 0.11	0.50 ± 0.05	0.36	0.48	–
02	20	19 42 54.82	23 18 59.6	4.40 ± 0.01	0.56 ± 0.01	0.18	0.44	0.78(G)
03	74	19 42 58.40	23 20 16.9	2.70 ± 0.01	0.53 ± 0.01	0.75	0.44	0.76(G)
04	73	19 43 01.60	23 20 37.7	0.53 ± 0.01	0.55 ± 0.01	0.10	0.21	–
05	18	19 42 59.58	23 17 45.9	3.65 ± 0.08	0.55 ± 0.03	0.59	0.81	0.28(G)
06	23	19 42 55.14	23 16 20.4	2.52 ± 0.01	0.58 ± 0.01	0.02	0.60	–
07	17	19 43 01.94	23 17 30.3	3.90 ± 0.01	0.54 ± 0.01	1.09	0.33	0.64(S)
08	78	19 43 02.76	23 18 22.8	3.58 ± 0.14	0.60 ± 0.04	2.68	0.44	0.73(G)
09	–	19 43 02.06	23 15 37.4	4.32 ± 0.08	0.53 ± 0.02	0.75	0.33	–
10	27	19 43 02.84	23 14 49.2	2.16 ± 0.02	0.58 ± 0.01	0.22	0.86	–
11	26	19 43 04.45	23 14 49.5	2.02 ± 0.02	0.51 ± 0.01	0.58	0.67	–
12	13	19 43 06.85	23 16 12.6	3.18 ± 0.03	0.54 ± 0.02	0.99	0.89	0.71(G)
13	28	19 43 01.53	23 14 40.8	3.83 ± 0.01	0.60 ± 0.01	0.02	0.53	–
14	75	19 43 05.01	23 19 50.0	2.25 ± 0.04	0.56 ± 0.03	0.65	0.19	–
15	77	19 43 05.17	23 19 37.9	1.72 ± 0.01	0.54 ± 0.01	0.03	1.20	–
16	76	19 43 04.49	23 18 49.4	3.28 ± 0.02	0.56 ± 0.01	0.69	0.67	–
17	16	19 43 06.03	23 17 33.1	3.37 ± 0.20	0.55 ± 0.07	1.33	0.29	0.32(G)
18	71	19 43 10.33	23 20 51.0	1.15 ± 0.14	0.50 ± 0.12	1.41	0.92	–
19	70	19 43 10.91	23 20 20.8	4.12 ± 0.01	0.51 ± 0.01	0.06	0.67	–
20	68	19 43 13.62	23 19 05.8	4.60 ± 0.02	0.51 ± 0.01	1.11	0.44	0.99(G)
21	12	19 43 09.60	23 16 35.3	0.70 ± 0.06	0.60 ± 0.08	0.69	1.13	0.06(G)
22	11	19 43 12.46	23 16 29.8	5.26 ± 0.03	0.52 ± 0.01	0.87	0.33	1.00(G)
23	4	19 43 14.28	23 17 18.5	0.55 ± 0.01	0.54 ± 0.01	0.01	0.05	0.08(G)
24	9	19 43 14.69	23 16 01.5	4.50 ± 0.04	0.49 ± 0.02	1.57	0.22	0.99(G)
25	8	19 43 15.52	23 16 41.0	1.85 ± 0.02	0.56 ± 0.03	0.48	1.62	0.27(G)
26	5	19 43 16.67	23 17 44.7	1.67 ± 0.15	0.52 ± 0.14	1.42	1.18	–
27	64a	19 43 16.98	23 19 48.7	3.44 ± 0.02	0.52 ± 0.01	0.15	0.50	–
28	65	19 43 18.91	23 18 45.6	5.15 ± 0.11	0.54 ± 0.03	0.84	0.76	0.92(G)
29	64	19 43 20.30	23 19 20.6	0.85 ± 0.02	0.52 ± 0.03	0.24	0.18	0.11(G)
30	62	19 43 22.55	23 18 26.6	1.44 ± 0.01	0.56 ± 0.01	0.02	0.25	1.28(E)
31	61	19 43 21.83	23 17 33.6	0.97 ± 0.01	0.51 ± 0.02	0.16	0.44	–
32	63	19 43 23.11	23 18 11.6	1.46 ± 0.03	0.54 ± 0.03	0.23	0.41	–
33	65a	19 43 16.90	23 17 26.6	1.28 ± 0.03	0.57 ± 0.04	0.22	0.06	–
34	–	19 43 22.96	23 15 14.7	1.07 ± 0.09	0.56 ± 0.13	0.88	0.52	–
35	25	19 43 02.04	23 15 49.5	3.82 ± 0.14	0.57 ± 0.08	1.43	0.36	0.71(G)
36	–	19 43 05.18	23 17 10.7	3.08 ± 0.01	0.50 ± 0.01	0.06	0.52	–
37	10	19 43 12.04	23 16 10.1	6.05 ± 0.07	0.50 ± 0.01	0.53	0.40	–
38	–	19 43 16.98	23 16 09.5	3.61 ± 0.02	0.52 ± 0.01	0.16	0.74	–
39	–	19 43 14.54	23 20 17.0	5.07 ± 0.05	0.53 ± 0.01	1.03	0.56	–
40	14	19 43 07.13	23 16 35.8	3.18 ± 0.12	0.55 ± 0.06	3.59	0.22	0.72(G)
41	33	19 43 16.05	23 13 22.0	1.05 ± 0.01	0.55 ± 0.01	0.05	0.36	0.71(S)
42	36	19 43 16.27	23 11 31.7	2.42 ± 0.01	0.56 ± 0.01	0.01	0.74	–
43	–	19 43 14.72	23 09 59.2	2.37 ± 0.02	0.53 ± 0.01	0.07	0.27	–
44	34	19 43 23.11	23 12 39.5	3.70 ± 0.01	0.54 ± 0.01	0.33	0.22	1.07(G)
45	51	19 43 28.70	23 14 38.5	2.07 ± 0.03	0.55 ± 0.03	0.40	1.00	–
46	53	19 43 32.51	23 15 04.9	1.86 ± 0.01	0.53 ± 0.01	0.02	0.36	–
47	35	19 43 29.37	23 10 39.7	1.59 ± 0.02	0.53 ± 0.02	0.62	0.22	0.79(S)
48	50	19 43 37.73	23 14 02.4	0.59 ± 0.01	0.57 ± 0.01	0.30	0.37	–
49	49	19 43 38.93	23 14 07.1	1.12 ± 0.04	0.50 ± 0.07	0.82	0.87	–
50	–	19 43 33.47	23 10 01.2	1.80 ± 0.01	0.58 ± 0.02	0.10	0.59	–
51	42	19 43 44.14	23 11 12.7	0.98 ± 0.01	0.56 ± 0.01	0.23	0.26	–
52	98	19 43 05.38	23 24 32.8	1.47 ± 0.02	0.59 ± 0.02	0.11	0.16	–
53	99	19 43 04.96	23 24 17.6	2.69 ± 0.10	0.50 ± 0.03	0.39	0.36	–
54	80	19 43 05.36	23 23 11.1	1.90 ± 0.08	0.57 ± 0.05	1.04	0.33	–
55	79	19 43 04.93	23 22 54.4	3.21 ± 0.01	0.55 ± 0.01	0.02	0.57	–
56	–	19 43 09.17	23 23 42.1	3.37 ± 0.01	0.55 ± 0.01	0.04	0.37	–
57	81	19 43 13.32	23 22 12.2	4.41 ± 0.22	0.51 ± 0.07	2.22	0.74	–
58	–	19 43 12.91	23 23 32.2	2.15 ± 0.08	0.54 ± 0.06	0.50	0.35	–
59	82	19 43 17.75	23 22 12.3	0.91 ± 0.01	0.52 ± 0.01	0.09	0.09	0.92(S)
60	125	19 43 20.03	23 25 42.1	0.71 ± 0.04	0.55 ± 0.10	1.16	0.21	–
61	–	19 43 21.66	23 24 08.7	2.77 ± 0.14	0.60 ± 0.08	0.98	0.35	–
62	–	19 43 23.35	23 23 29.7	0.66 ± 0.01	0.59 ± 0.03	0.31	0.33	–

Table 4 – *continued*

ID(M)† (1)	ID(B)†† (2)	RA(2000J) (3)	Dec.(2000J) (4)	$P_{\max} \pm \epsilon$ (per cent) (5)	$\lambda_{\max} \pm \epsilon$ (μm) (6)	σ_1 (7)	$\bar{\epsilon}$ (8)	$E(B-V)$ (9)
63	96	19 43 24.02	23 23 19.2	1.74 ± 0.04	0.51 ± 0.03	0.20	0.33	–
64	–	19 43 24.83	23 26 14.7	3.01 ± 0.12	0.51 ± 0.04	0.50	0.24	–
65	–	19 43 26.47	23 26 21.1	4.97 ± 0.07	0.53 ± 0.02	0.36	0.53	–
66	–	19 43 26.27	23 20 33.3	1.65 ± 0.02	0.51 ± 0.02	0.14	0.40	–
67	88	19 43 28.09	23 21 13.0	0.71 ± 0.01	0.52 ± 0.04	0.46	0.15	–
68	–	19 43 30.17	23 21 19.4	1.39 ± 0.01	0.50 ± 0.01	0.10	0.17	–
69	86	19 43 31.42	23 20 40.3	1.11 ± 0.11	0.51 ± 0.11	0.76	0.11	–
70	127	19 43 28.34	23 24 34.1	3.38 ± 0.02	0.58 ± 0.01	1.10	1.67	–
71	130	19 43 30.70	23 25 29.0	1.23 ± 0.01	0.59 ± 0.03	0.20	0.58	–
72	129	19 43 29.84	23 25 10.7	4.09 ± 0.07	0.50 ± 0.02	0.44	0.56	–
73	95	19 43 31.27	23 23 08.5	1.43 ± 0.01	0.55 ± 0.02	0.36	0.57	0.52(G)
74	93	19 43 32.43	23 22 09.7	2.75 ± 0.01	0.50 ± 0.01	0.31	0.67	0.64(G)
75	94	19 43 32.95	23 22 41.6	3.01 ± 0.13	0.51 ± 0.04	0.43	0.83	–
76	91	19 43 36.55	23 21 08.5	3.19 ± 0.02	0.55 ± 0.01	0.48	0.56	0.79(S)
77	–	19 43 40.13	23 25 41.3	1.29 ± 0.01	0.49 ± 0.01	0.14	0.60	–
78	–	19 43 41.07	23 24 44.0	1.59 ± 0.08	0.49 ± 0.04	0.48	1.17	–
79	–	19 43 42.50	23 24 42.7	2.21 ± 0.14	0.59 ± 0.07	0.66	0.48	–
80	–	19 43 11.95	23 24 50.7	3.49 ± 0.06	0.57 ± 0.02	0.32	0.72	–
81	128	19 43 30.09	23 24 34.4	4.25 ± 0.06	0.56 ± 0.02	0.52	0.24	–
82	–	19 43 24.58	23 21 15.3	0.95 ± 0.05	0.51 ± 0.07	0.40	0.42	–
83	–	19 42 25.70	23 16 16.3	1.41 ± 0.11	0.53 ± 0.12	1.41	0.83	–
84	–	19 42 28.22	23 16 18.4	1.19 ± 0.01	0.50 ± 0.02	0.26	0.67	–
85	–	19 42 29.26	23 13 50.4	0.77 ± 0.01	0.55 ± 0.02	0.66	0.75	–
86	–	19 42 31.16	23 15 00.4	2.83 ± 0.03	0.57 ± 0.02	0.09	0.26	–
87	–	19 42 32.97	23 17 33.5	3.69 ± 0.01	0.52 ± 0.01	0.16	1.33	–
88	–	19 42 35.12	23 16 27.4	2.46 ± 0.01	0.53 ± 0.01	0.02	1.25	–
89	–	19 42 36.55	23 11 22.3	3.38 ± 0.03	0.57 ± 0.02	0.16	0.33	–
90	–	19 42 38.92	23 13 43.4	4.34 ± 0.07	0.57 ± 0.03	0.40	0.93	–
91	–	19 42 40.51	23 14 38.1	3.26 ± 0.02	0.52 ± 0.02	0.25	0.47	–
92	184	19 42 41.38	23 14 41.3	3.29 ± 0.07	0.51 ± 0.03	0.67	0.67	–
93	179	19 42 42.33	23 16 57.6	1.98 ± 0.05	0.53 ± 0.03	0.51	0.57	0.93(E)
94	180	19 42 42.79	23 16 39.5	2.57 ± 0.01	0.52 ± 0.01	1.10	0.22	–
95	–	19 42 40.72	23 11 18.6	2.57 ± 0.05	0.50 ± 0.02	0.24	0.61	–
96	191	19 42 45.20	23 13 15.9	2.68 ± 0.08	0.53 ± 0.04	0.51	0.33	–
97	–	19 42 45.58	23 14 15.0	2.28 ± 0.01	0.57 ± 0.03	0.16	0.76	–
98	185	19 42 46.19	23 15 02.0	2.88 ± 0.01	0.52 ± 0.01	0.08	0.74	–
99	22	19 42 50.25	23 18 25.4	2.28 ± 0.01	0.52 ± 0.01	0.03	0.13	–
100	186	19 42 50.32	23 15 39.1	3.77 ± 0.01	0.55 ± 0.01	0.32	0.67	–
101	192	19 42 50.17	23 12 45.2	2.81 ± 0.07	0.51 ± 0.04	0.72	1.83	–
102	187	19 42 56.48	23 13 37.9	3.26 ± 0.09	0.55 ± 0.08	4.66	0.44	–
103	–	19 43 02.16	23 16 14.1	4.22 ± 0.01	0.51 ± 0.01	0.02	0.21	–
104	29	19 43 02.13	23 14 30.4	4.39 ± 0.05	0.50 ± 0.02	1.28	0.33	–

† According to this observation.
†† According to Barkhatova (1957).
(G) According to Guetter (1992)
(S) According to Stone (1988)
(E) According to Erickson (1971).

Out of 104 stars observed by us, only for one non-member star (namely #57M) and three member stars (namely #08M, #40M and #102M) is the value of σ_1 above the limit of 1.6. The dispersion in the position angle $\bar{\epsilon}$ is found to be higher for one member star (namely #25M) and eight non-member stars (namely #15M, #21M, #45M, #70M, #78M, #87M, #88M and #101M). The $\lambda_{\max}$ for the above-mentioned 13 stars detected using the two criteria σ_1 and $\bar{\epsilon}$ is nearly equal to that for the interstellar medium, except in the case of non-member star #78M. Star #78M is found to have a lower value of $\lambda_{\max}$ and a higher value of $\bar{\epsilon}$, but its σ_1 is lower than the threshold. Therefore, the polarization towards NGC 6823 is found to be due mainly to foreground interstellar dust grains.

If the polarization is mainly dominated by dust particles present in the diffuse interstellar medium, the value of $\lambda_{\max}$ should be nearly equal to 0.55 ± 0.04 μm. The weighted mean of $\lambda_{\max}$ for the observed member and non-member stars of NGC 6823 is obtained as 0.53 ± 0.01 μm and 0.54 ± 0.01 μm, respectively. The similarity in values of $\lambda_{\max}$ for the member and non-member stars implies that the light from both member and non-member stars encounters the same population of foreground dust grains. Therefore, the characteristic grain-size distribution as indicated by the polarization study of stars in NGC 6823 is nearly the same as that for the general interstellar medium. The weighted mean of maximum polarization for the member and

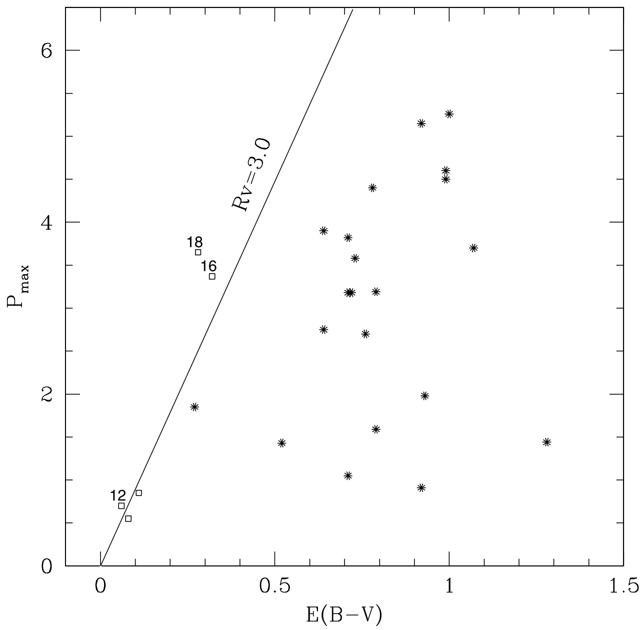

Figure 10. Polarization efficiency diagram, with the line of maximum efficiency drawn using $R_V = 3.0$. The stars observed by us in the direction of NGC 6823 are shown using open black square. The stars with $M_P \geq 0.50$ are identified using asterisks.

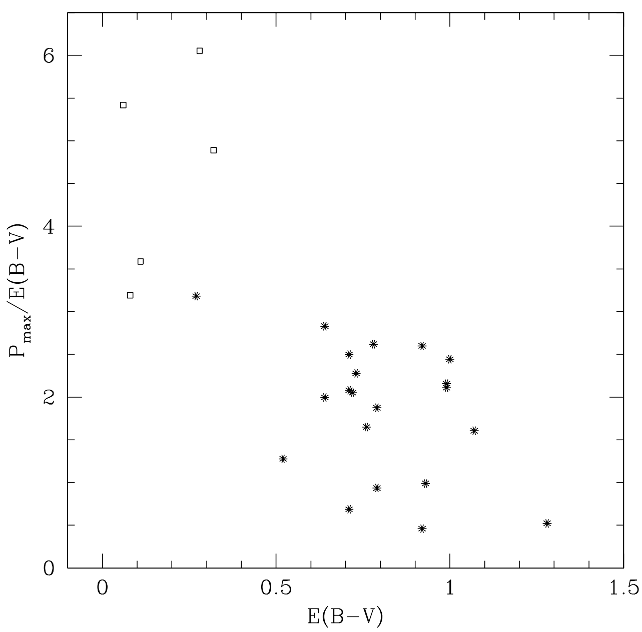

Figure 11. $P_{max}/E(B-V)$ plotted as a function of $E(B-V)$. The stars observed by us in the direction of NGC 6823 are shown using open black squares. The stars with $M_P \geq 0.50$ are identified using asterisks.

non-member stars is found as 2.82 ± 0.01 per cent and 1.76 ± 0.01 per cent, respectively.

3.3 Polarization efficiency

For interstellar dust particles in a diffuse interstellar medium, the ratio between the maximum amount of polarization and the visual extinction (polarization efficiency) cannot exceed the empirical upper limit (Hiltner 1956)

$$P_{max} < 3A_V \simeq 3R_V \times E(B-V). \tag{6}$$

The ratio $P_{max}/E(B-V)$ depends mainly on the alignment efficiency, magnetic strength and amount of depolarization due to radiation traversing more than one cloud in different directions.

Fig. 10 shows the relation between the colour excess $E(B-V)$ and maximum polarization P_{max} for the stars observed by us (open squares for non-member and asterisks for member stars) towards NGC 6823, produced by the dust grains along the line of sight to the cluster. Out of the 104 stars observed by us, $E(B-V)$ is available only for 26 stars (21 member and five non-member stars). In the polarization-efficiency diagram, three non-member stars #12, #16 and #18 (identification according to ID(B)) are lying to the left side of the interstellar maximum line, which implies that these three stars may be affected by intrinsic polarization. In case of star #12, the dispersion in the position angle $\overline{\epsilon}$ is found to be higher (1.13) but σ_1 is lower than the threshold. Apparently, the dominant mechanism of polarization for the observed member stars of NGC 6823 is selective absorption by interstellar dust grains that are aligned by the local and Galactic magnetic fields. Fig. 10 also indicates that, while the colour excess for the member stars of NGC 6823 varies from 0.27–1.28 mag approximately, the variation in the polarization value is very high, ∼4.5 per cent. The high variation of P_{max} indicates that different populations of dust grains may be present in the line of sight towards NGC 6823, as inferred from Section 3.1.

In Fig. 11, we plot $P_{max}/E(B-V)$ versus $E(B-V)$ for the 104 stars observed by us with available colour excess $E(B-V)$ (black open squares for non-member stars and asterisks for member stars). The polarization efficiency is found to fall with increasing $E(B-V)$. The decrement of polarization efficiency with increasing $E(B-V)$ may be due to an increase in the size of the dust grains or a small change in the polarization position angle.

4 SUMMARY

The main results of this study are summarized as follows.

We have observed the linear polarization of 104 stars in the region of the open cluster NGC 6823. The analysis of these data shows that the polarization is mostly due to foreground dust grains distributed in a patchy pattern, and the majority of the observed stars do not present an indication of intrinsic polarization. We also found evidence of several dust layers/components along the line of sight to the cluster. Combining our results with those from the literature, we present evidence for the presence of a first layer of dust located approximately within 200 pc towards the cluster.

The radial distribution of the position angles for the member stars is found to show a systematic change, while the polarization is found to reduce towards the outer parts of the cluster. The average position angle of the member stars belonging to the coronal region is closer to the inclination of the Galactic parallel (∼32°) than the nuclear region of the cluster.

The polarization efficiency for the cluster member stars is quite similar to that for field stars, which implies that a similar polarization mechanism is responsible for both member and field stars towards the cluster.

The weighted means of maximum wavelength λ_{max} for the cluster members and the field stars are found to be 0.53 ± 0.01 μm and 0.54 ± 0.01 μm, respectively. These values of λ_{max} for stars towards NGC 6823 are thus similar to those of the interstellar medium (0.55 ± 0.04 μm). Therefore the polarization towards NGC 6823 is caused mainly by foreground dust grains, as we have already inferred for clusters IC 1805 and NGC 654 (Medhi et al. 2007; Medhi et al. 2008). The intracluster dust grains are very similar to those of the general interstellar medium.

ACKNOWLEDGMENTS

The authors thank the referee, Professor Carlos Feinstein, for his constructive comments and suggestions which have led to substantial improvements in the paper. It is also our pleasure to thank Prof H. C. Bhatt for his useful suggestions. This research has made use of the WEBDA data base, operated at the Institute for Astronomy of the University of Vienna; use of images from the National Science Foundation and Digital Sky Survey (DSS), which was produced at the Space Telescope Science Institute under the US Government grant NAG W-2166. This research also made use of NASA's Astrophysics Data System and IRAF, distributed by National Optical Astronomy Observatories, USA. BJM thanks his daughter Sanskriti and wife Orchid for their support.

REFERENCES

Barkhatova K. A., 1957, SvA, 1, 827
Chapin E. L. et al., 2008, ApJ, 681, 428
Clayton G. C., Cardelli J. A., 1988, AJ, 96, 695
Corradi R. L. M., Aznar R., Mampaso A., 1998, MNRAS, 297, 617
Coyne G. V., Magalhaes A. M., 1979, AJ, 84, 1200
Dame T. M., Thaddeus P., 1985, ApJ, 170, 325
Davis L. J., Greenstein J. L., 1951, ApJ, 114, 206
Dias W. S., Assafin M., Flório V., Alessi B. S., Líbero V., 2006, A&A, 446, 949
Dobashi K., Uehara H., Kandori R., Sakurai T., Kaiden M., Umemoto T., Sato F., 2005, PASJ, 57, 1
Erickson R. R., 1971, A&A, 10, 270
Feinstein A., 1994, Rev. Mex. Astron. Astrofis., 29, 141
Fresneau A., Monier R., 1999, AJ, 118, 421
Guetter H. H., 1992, AJ, 103, 197
Hall J. S., 1958, Publ. US Naval Obser., 17, 1
Heiles C., 2000, AJ, 119, 923
Hiltner W. A., 1956, ApJS, 2, 389
Hoag A. A., Johnson H. L., Iriarte B., Mitchell R. I., Hallam K. L., Sharpless S., 1961, Publ. US Naval Obser., 17, 343
Høg E. et al., 1997, A&A, 323, 57
Kharchenko N. V., Piskunov A. E., Rser S., Schilbach E., Scholz R. D., 2005, A&A, 438, 1163
Lazarian A., Goodman A. A., Myers P. C., 1997, ApJ, 490, 273
Leisawitz D., Bash F. N., Thaddeus P., 1989, ApJS, 70, 731
Lynds B. T., 1962, ApJS, 7, 1
McMillan R. S., 1978, ApJ, 225, 880
Medhi B. J., Maheswar G., Brijesh K., Pandey J. C., Kumar T. S., Sagar R., 2007, MNRAS, 378, 881
Medhi B. J., Maheswar P. J. C., Kumar T. S., Sagar R., 2008, MNRAS, 388, 105
Morgan W. W., Whitford A. E., Code A. D., 1953, ApJ, 118, 318
Neckel Th., Klare G., 1980, A&AS, 42, 251
Orsatti A. M., Vega E., Marraco H. G., 1998, AJ, 116, 266
Pandey J. C., Medhi B. J., Sagar R., Pandey A. K., 2009, MNRAS, 396, 1004
Perryman M. A. C. et al., 1997, A&A, 323, 49
Ramaprakash A. N., Gupta R., Sen A. K., Tandon S. N., 1998, A&AS, 128, 369
Rautela B. S., Joshi G. C., Pandey J. C., 2004, Bull. Astron. Soc. India, 32, 159
Sagar R., 1987, MNRAS, 228, 483
Sagar R., Joshi U. C., 1981, Ap&SS, 75, 465
Schmidt G. D., Elston R., Lupie O. L., 1992, AJ, 104, 1563
Serkowski K., 1965, ApJ, 141, 1340
Serkowski K., 1973, in Greenberg J. M., van de Hulst H. C., eds, IAU Symp. 52, Interstellar Dust and Related Topics. Reidel, Dordrecht, p. 145
Serkowski K., Mathewson D. L., Ford V. L., 1975, ApJ, 196, 261
Spitzer L., 1978, Physical processes in the interstellar medium. John Wiley & Sons, New York
Stone R. C., 1988, AJ, 96, 1389
Turner D. G., 1979, J. R. Astron. Soc. Canada, 73, 74
Turnshek D. A., Bohlin R. C., Williamson R. L., II, Lupie O. L., Koornneef J., Morgan D. H., 1990, AJ, 99, 1243
Whittet D. C. B., 1992, Dust in the Galactic Environment. IOP, Bristol
Whittet D. C. B., van Breda I. G., 1978, A&A, 66, 57
Wilking B. A., Lebofsky M. J., Kemp J. C., Martin P. G., Rieke G. H., 1980, ApJ, 235, 905
Wilking B. A., Lebofsky M. J., Rieke G. H., 1982, AJ, 87, 695

This paper has been typeset from a TEX/LATEX file prepared by the author.